Underground Design Methods 2015 – Y Potvin (ed.)

doi:10.36487/ACG_rep/1511_06_Earl

Study of stress conditions at Williams Mine using underground observations and microseismic monitoring data

PJ Earl *Global Mine Design Ltd, UK*

D Malovichko *Institute of Mine Seismology, Australia*

D Rebuli *Institute of Mine Seismology, Canada*

Abstract

The C Zone/Interlake orebody at Williams Mine, Ontario, Canada, is one of the Hemlo ore-bearing lodes. It is adjacent to the B Zone orebody, for which the stress state has been well studied, with evidence supported by underground observations. The extrapolation of stress conditions from B Zone to C Zone/Interlake seemed logical, thus common characteristics of in situ stress were previously used for design and planning purposes. Over time, a number of discrepancies were found between the assumed stress state and underground observations (damage of boreholes and orepasses) around the C Zone/Interlake orebody.

An alternative model of in situ stress was considered for the C Zone/Interlake region. The induced stresses were evaluated for a mining sequence for both old and new models. The recorded seismic response to the modelled sequence was compared with the expected response in terms of location and source mechanisms of seismic events. The new model shows better agreement, increasing confidence in numerical stress models used for C Zone/Interlake mine planning.

1 Introduction

Williams Mine is part of the historic Hemlo gold mining complex situated approximately 1,100 km northwest of Toronto in Ontario, Canada, which is now solely operated by Barrick Gold Corporation. The C Zone orebody is situated west of the better-known B Zone orebody.

The C Zone orebody was first accessed in 2004, and although reported as more structured with discontinuities comprising a higher percentage of weak infill material (Bawden 2006), ground conditions were generally considered similar to the B Zone with three major discontinuity sets present (Table 1). Due to the orebodies similarities, B Zone stress conditions, first defined by Kazakidis (1990) and later refined by Coulson (2009), were adopted for mine planning purposes; see Figure 1 and Table 2.

C Zone mining subsequently began using B Zone mining methods of longhole and alimak stopes. Level infrastructure was laid out in the same manner as B Zone, with footwall haulage drives orientated parallel to foliation comprising a shanty back profile to accommodate C set discontinuities, and square profile orebody access drifts orientated parallel to B set discontinuities.

With steady orebody development and inclusion of the Interlake down-dip extension below 9,450 mRL, C Zone accounted for 80% of total underground production by September 2009. However, by late 2010, a number of large-scale ground failures in both infrastructure and production areas had occurred throughout the C Zone and Interlake mine regions that could not be reconciled between comparisons of underground observations and results of numerical stress modelling using B Zone stress assumptions.

The C Zone/Interlake orebody were forecast to account for 100% of Williams Mine underground production from 2011 onwards; therefore, increased importance was placed on properly characterising stress conditions for the purpose of mine planning. This paper describes observations that led to the recognition of different stress conditions in C Zone/Interlake and some of the validation methods used.

Table 1 Williams Mine general structural conditions

Discontinuity set	Relative to orebody grid north			Mine infrastructure
	Strike	Dip	Dip direction	
A ('foliation')	East–west	Moderate	North	FW haulage drives
B	North–south	Vertical	–	Ore access drifts
C	East–west	Shallow	South	Shanty for FW haulage drives

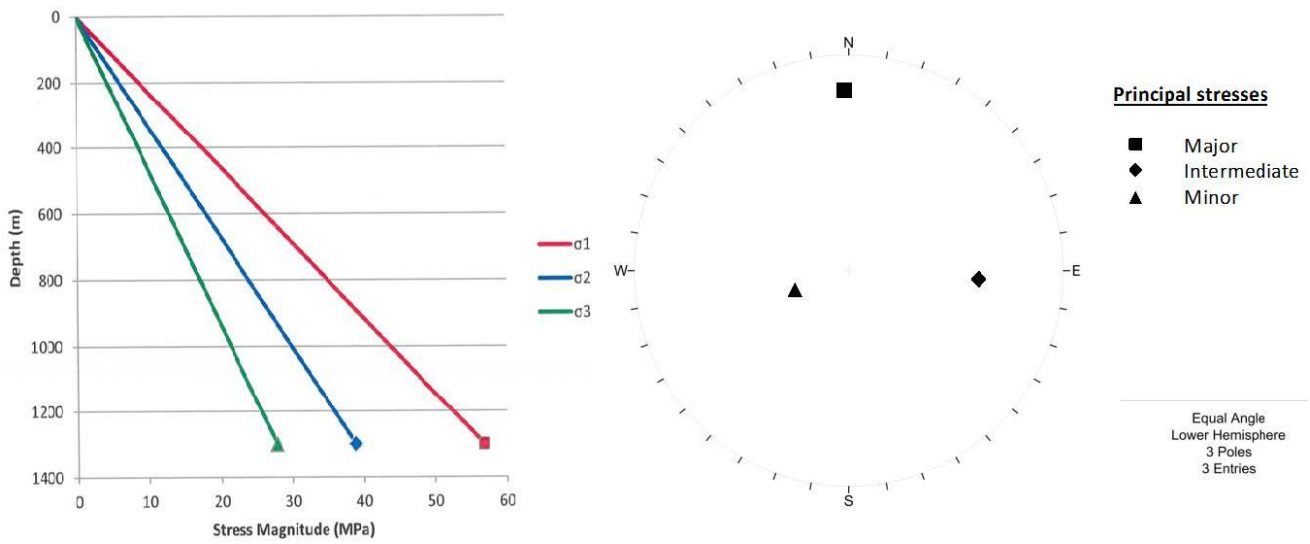

Figure 1 B Zone stress conditions (after Coulson 2009) — with respect to B Zone mine grid

Table 2 Summary of B Zone stresses (after Coulson 2009) — with respect to B Zone mine grid

Principal stress	Trend (°)	Plunge (°)	Magnitude (MPa/metre)
σ_1	358	10	0.0437
σ_2	093	28	0.0299
σ_3	250	60	0.0214

Note: surface elevation is generally assumed to be 10321.5 m RL.

2 Initial work on re-characterising stresses

2.1 Initial indicators of different conditions in C Zone

The earliest indications of unusual C Zone/Interlake stress conditions were simple yet astute observations made during underground inspections. Separation of normally tight discontinuity planes in pillars and spalling rock from the lower sections of rib pillars between ore drives started to occur during the level development phase, well before stoping commenced on the level, and at much lower block extraction ratios than anticipated from previous experience gained from mining the B Zone orebody.

In addition, stress arching was noted in the overcut back of the very first Interlake stope, 9410-140-27, as shown in Figure 2. This stope was at least 200 m below the nearest active mining block and surrounded only by level development. The stress arching implied that the major principal stress was acting across the orebody, in a west to east direction, which did not agree with the major principal stress acting through the orebody from north to south, as assumed from B Zone experience.

Figure 2 9410-140-27, stope overcut showing stress arching (looking towards hanging wall contact)

2.2 Geological review and standardisation of Hemlo data

The structural complexity of the C Zone orebody was placed into context by a full review of the Hemlo regional geology. Figure 3 shows that the Hemlo gold deposits lie within complex faulted and folded intermediate meta-intrusive rocks and that C Zone has been rotated by folding when compared to historical Hemlo orebodies (Williams B Zone, Golden Giant and David Bell). The labels 'B Zone (Hemlo main zone)' and 'C Zone 300 series' indicate the different orebody orientations. The headframe locations of each Hemlo mine are also shown.

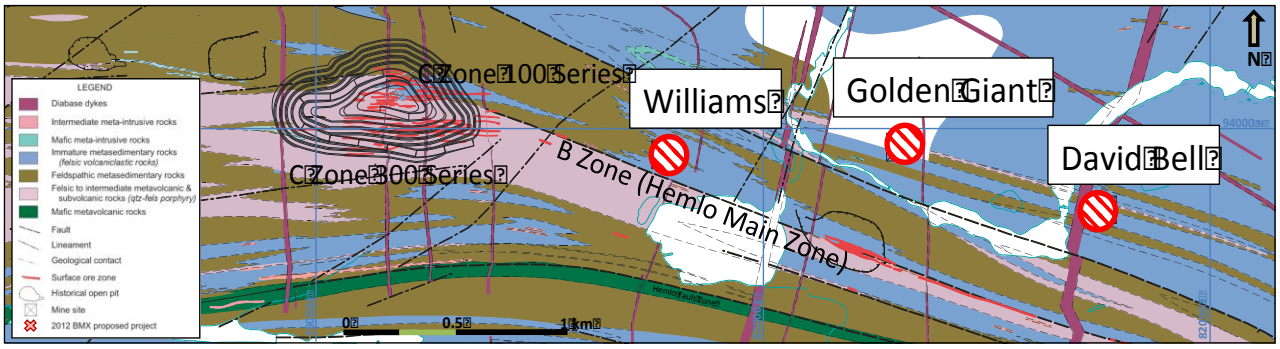

Figure 3 Hemlo mines regional geology (after Muir 1997) orientated to Universal Transverse Mercator (UTM) coordinate system grid north

Identification of the difference in orebody orientation between C Zone/Interlake and B Zone also highlighted a critical oversight in ongoing C Zone mine planning and design. Historically, B Zone, Golden Giant and David Bell used more or less the same survey grid, in which local north was rotated to be perpendicular to the orebody strike to allow levels to be laid out on an orthogonal grid; for Williams Mine this is referred to as the B Zone Grid. When C Zone production began, the rotated orebody was accommodated by the creation of a second mine grid, on which grid north was orientated perpendicular to C Zone orebody strike. The C Zone grid is a truncated version of UTM, with the difference of 17°11'50" between C Zone and B Zone grid north.

Although this finding seems relatively straightforward, it was not explicitly explained in mine design documentation prior to 2011. Technical staff produced production plans for the two Williams Mine orebodies separately in the respective grid systems and over time the acceptance of two separate survey standards reduced understanding of the significance of this information.

Realising the need for more explicit mine planning rules between B Zone and C Zone, the geotechnical team embarked on a project to define C Zone conditions by transposing all historical Hemlo production data, including geological and geotechnical data, into one 'whole of Hemlo' 3D-model environment. The B Zone mine grid was chosen as the common survey system so that historical data from all three Hemlo mine properties could be included. All stopes from the near 30-year production history of the three mines were re-created in computer software with the B Zone, Golden Giant and David Bell stopes correctly sequenced to an accuracy of one month for historical purposes; C Zone stopes were sequenced stope by stope.

A large database was also created containing temporally correct production data for each C Zone stope, such that the status could be recalled for any time period in question. This exercise took several months to complete, but resulted in a vast array of data that could be investigated in the course of verifying the C Zone orebody environment.

2.3 Seismic system upgrade

In July 2013, a single, state-of-the-art Institute of Mine Seismology (IMS) seismic system was installed throughout the three Hemlo mines. This was tied to the model environment previously described, and replaced several older-generation Engineering Seismology Group (ESG) systems that were not linked together. Lower frequency triaxial geophone sensors were added to new and existing sensor arrays for the collection of seismic event source parameters. The initial system calibration focused first on the new IMS geophone sensors and, following a series of back-analyses and additional calibration blasts, it was also possible to confirm orientation and polarity of high-frequency uniaxial accelerometers from the original systems. This upgrade allowed routine quantitative seismology to be carried out on seismic events throughout the Hemlo camp.

The analyses described in this paper were part of a series of evaluations on seismic events recorded throughout the three underground mines (Williams, Golden Giant and David Bell) in the period from July 2013 to August 2014. Source mechanisms were obtained for events that were of sufficient signal/noise ratio, and generally recorded by at least nine sensor sites with at least seven valid P-picks and seven valid S-picks. A moment tensor inversion algorithm that utilises polarities and amplitudes of both P-waves and S-waves was applied to get the mechanisms (Mendecki 1993; Malovichko & Lötter 2008).

2.4 Failure of Orepass 7

Orepass 7 (OP7) is the main C Zone orepass, situated slightly to the east of the C Zone orebody between 10,030 and 9,175 mRL where it connects to automated ore handling infrastructure. Failure of OP7 occurred above the orepass dump at 9,640 mRL, in March 2008, rendering the pass unusable below this section until the next dump at 9,450 mRL. The failure was an unusual shape, but occurred very early in the life of the pass; a geological investigation postulated the cause to be a poor quality geological structure.

A new location, approximately 20 m south and west of OP7, was selected and a bypass orepass (referred to as OP7A) was driven to replace the failed section of OP7 above 9450 mRL. OP7A subsequently failed in December 2010 around 9,765 mRL, with a similar shape, but no record of large-scale structures was present.

OP7 and OP7A failures both elongated from northwest to southeast with respect to B Zone mine grid, which in the absence of a reliable geological cause infers stress-induced failure where the major principal stress direction is sub-parallel to the C Zone orebody towards the northeast. However, historical stress-induced failures of B Zone orepasses (for example Orepass 5 (OP5) in 2003) strike west to east, which agrees with the expected major principal stress direction to the north, as shown in Figure 1. Figure 4 demonstrates the difference in orientation of the OP7/OP7A (C Zone) failures with that of OP5 (B Zone).

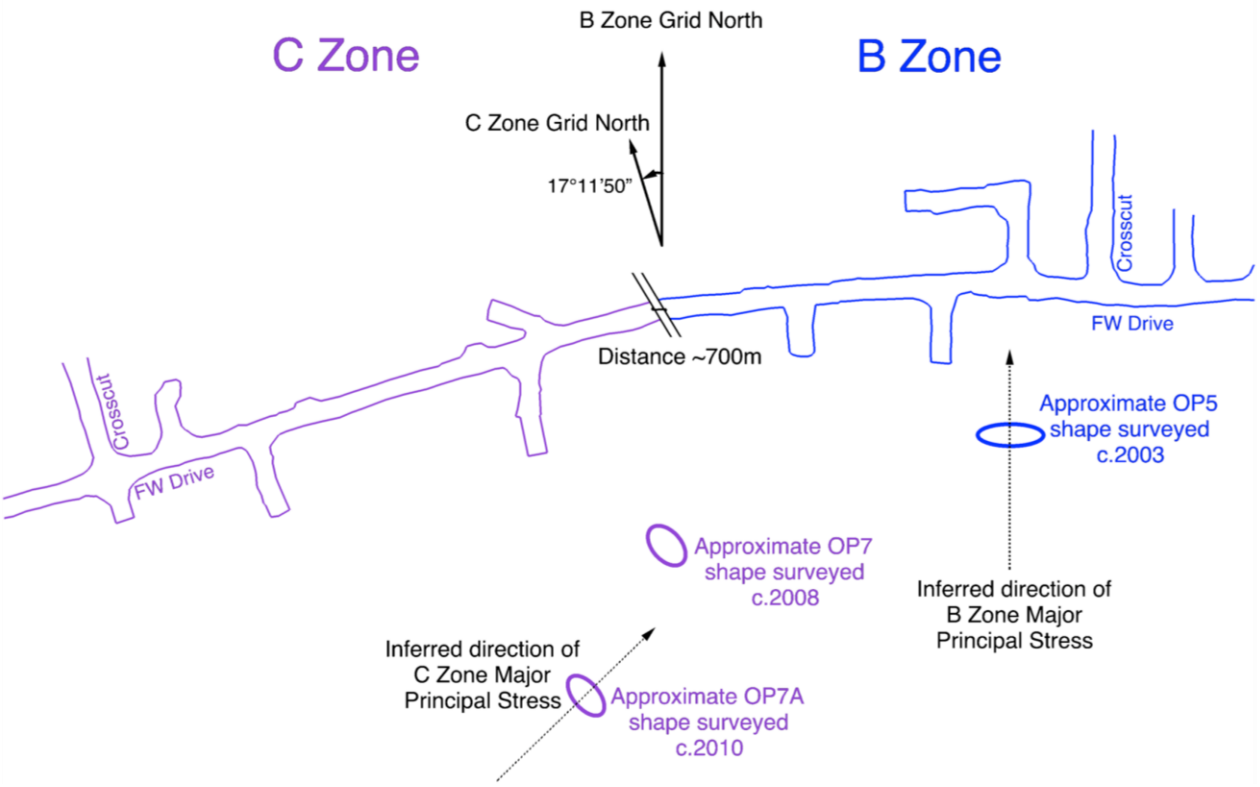

Figure 4 Comparison of orepass failure orientation between B Zone and C Zone

OP7 and OP7A continued to be the principal means of moving C Zone ore, through use of a 'pass to pass' rehandle at 9,640 mRL to avoid the respective failures. In November 2013, a significant increase in the number of seismic events was recorded around OP7 below 9,450 mRL, which prompted an investigation to determine what information the seismic events could provide on the rock mass condition surrounding the orepass.

Seismic events recorded around an orepass can be associated with either the mechanical impact of transported rocks (referred to as Type (A) events), or occur through stress fracturing of the rock mass surrounding the orepass (referred to as Type (B) events). Usually, Type (A) events produce seismic signals with lower frequencies as compared to Type (B) events; the difference in frequency can be described by the seismic parameter energy index (EI), (van Aswegen 1993).

The left hand image of Figure 5 shows all seismic events recorded around OP7 between November 2013 and January 2014, coloured by Log Energy Index limited within the range -1.0 (blue/top of legend) to +1.0 (red/bottom of legend). No particular pattern is revealed; some events have high energy index, while others do not.

To further understand the nature of events around the orepass, data filtering was increased to only include events recorded by more than 11 sensors and with moment magnitude greater than -0.8. Initially, a total of 14 events were used. Seven of the investigated source mechanisms were described by a single force mechanism with positive downward impulse; the remaining seven were described by moment tensor solution. The single force mechanism/positive vertical component events correspond to mechanical impact of rocks (Type (A) events) and are shown as smaller solid-coloured spheres in the right hand image of Figure 5; the remaining seven events correspond to stress fracturing (Type (B) events) and the resolved moment tensor solutions are shown as larger 'beach balls'.

Axis lines protruding from the beach balls are also visible, which correspond to seismic P-axes (proxy of σ_1). Note that these are approximately parallel with the strike of the C Zone orebody, with similar orientation to the OP7/OP7A failures.

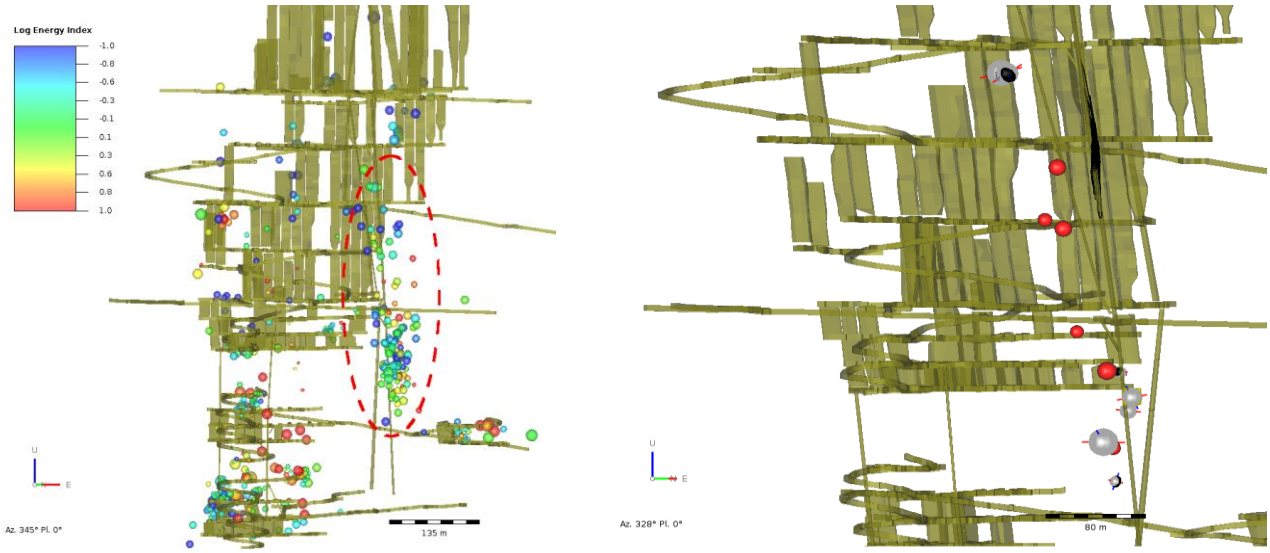

Figure 5 Seismic events recorded around OP7, up to January 2014, prior to OP7 failure below 9,450 mRL

The increased seismic activity in OP7 below 9,450 mRL led to orepass failure at this location in February 2014 and source mechanism analysis was repeated on events covering the time period from November 2013 up to failure. A total of 87 events were used in the second analysis with the same higher order filters as previously applied. Figure 6 shows the moment tensor solutions of this later set of analyses (left-hand image), which confirm that the P-axes (proxy of σ_1) are parallel to the C Zone orebody strike and perpendicular to the orepass failure shape determined by Cavity Monitoring Survey (right-hand image).

The precision of seismic event location around the orepass, and the agreement in direction of the P-axes, provided confidence that the source mechanism analysis technique was appropriate for use on C Zone/Interlake data. The results also confirmed that the previous OP7/OP7A failures were most likely stress related, and that the direction of major principal stress in this region agreed with the earlier observations of rock mass damage elsewhere in C Zone/Interlake.

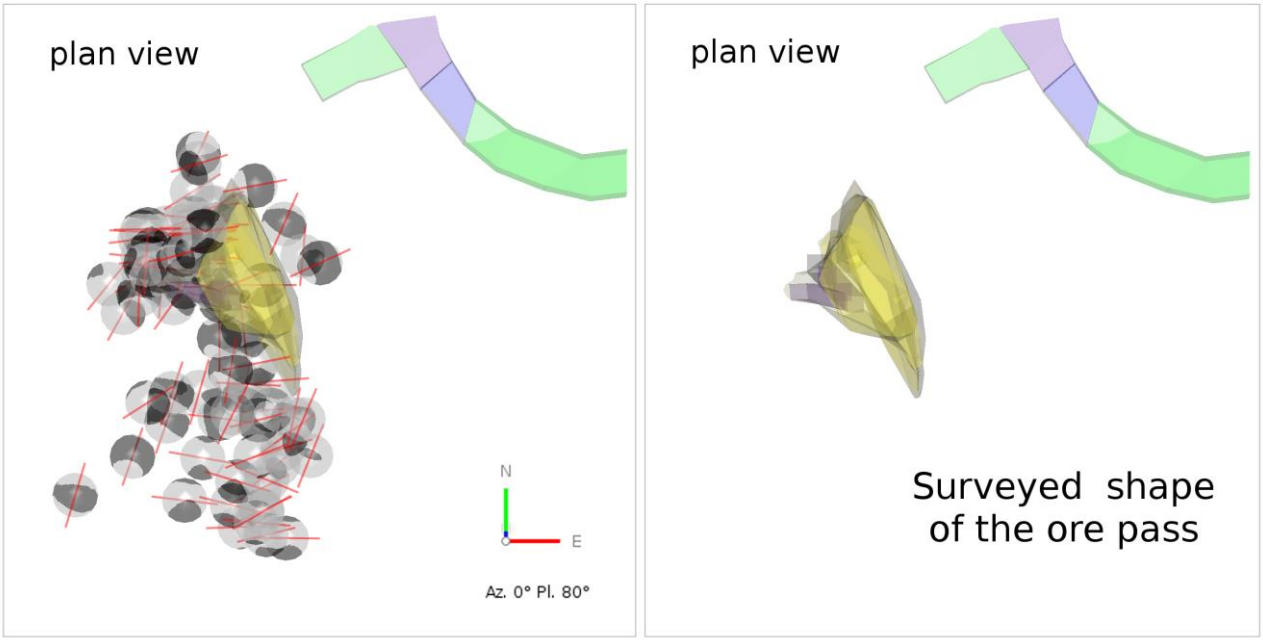

Figure 6 Correlation between seismic data (location and source mechanisms) recorded around OP7 below 9,450 mRL and the surveyed shape of the orepass

2.5 Stress tensor by underground observations

Simultaneously, two areas of the Interlake mining region were approaching a sill pillar extraction phase and observations of high induced-stresses manifesting within the mining levels led directly to the formation of a qualitative stress tensor to use in C Zone stress modelling analysis.

The direction of the major principal stress (σ_1) inferred from the moment tensor analysis in Section 2.4 was confirmed from observations made during longhole slot blasts. A typical slot blast sequence is shown in the left hand image of Figure 7 and an observed blasthole closure seen in Ring B, which was immediately behind the fully blasted slot, is shown in the right hand image. The azimuth of closure agrees with the average direction resolved from the seismic proxies of σ_1 detailed in Section 2.4. Note that the left hand image looks towards C Zone west and the top of the right image is C Zone north.

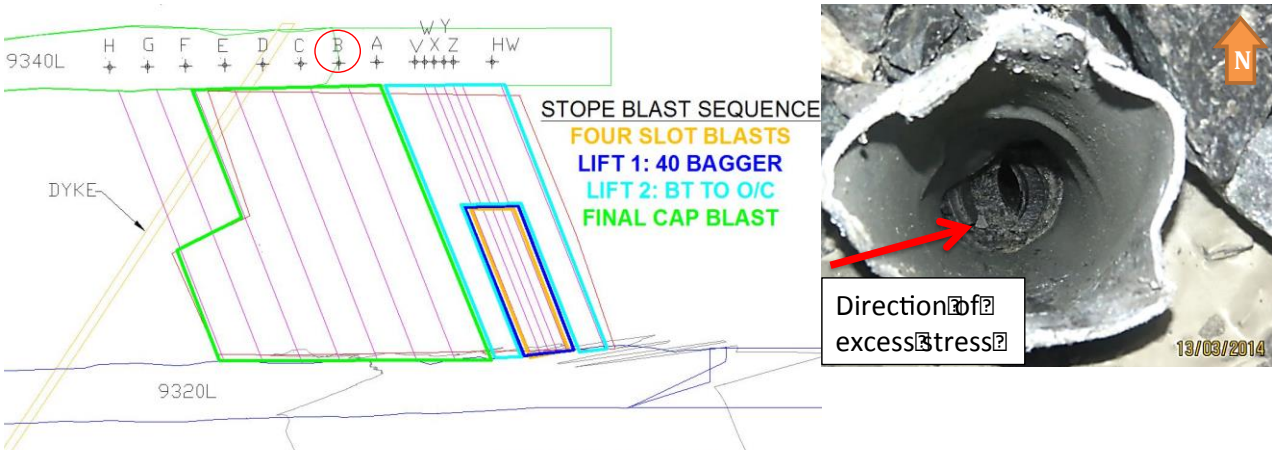

Figure 7 Typical Interlake longhole stope blast sequence and closure seen in Ring B behind fully blasted slot

Excess stress down-dip of the orebody was also noted in various horizontal drill holes within the sill pillar region. Figure 8 shows typical borehole breakout observed in an abutment of one of the Interlake sill pillars. The hole is horizontal, facing northeast with respect to B Zone mine grid and parallel to C Zone orebody strike; the stress direction is highlighted by an arrow. Due to the frequency at which breakout was observed throughout the Interlake mining region, this stress was considered to be the Intermediate principal stress (σ_2).

Figure 8 Borehole breakout (hole facing directly east along C Zone orebody strike)

The minor principal stress (σ_3) was interpreted from dilation of a series of discontinuities during stoping within the Interlake sill pillars. The discontinuities were recorded as absolutely planar with very long persistence, dipping at 20°S with respect to C Zone grid as shown in Figure 9(b). This fracture set is closely related to the C set discontinuities, which are a common characteristic of the C Zone orebody; however, undisturbed examples of C set discontinuities are undulatory, whereas discontinuities in active mining areas were always dead planar. In addition, in particularly advanced sill pillar mining areas, formation of these planes was picked up on the seismic system, as shown in Figure 9(a). Towards the end of 2014, when development had progressed to the footwall drive of the last sill level between mining blocks, overbreak from the drive back also began to occur along these planes in freshly blasted footwall haulage development headings.

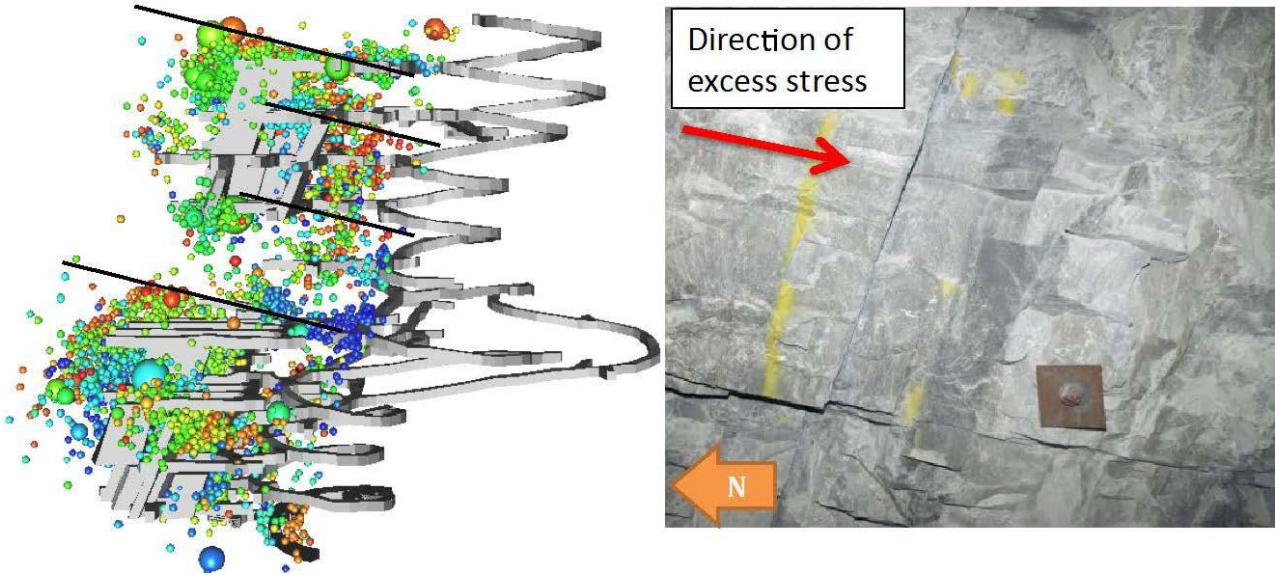

(a) (b)

Figure 9 (a) formation of fractures as seen from seismic system; and (b) close up of stress induced fracturing. Both are viewed towards the east

Evidence of the same three excess stress directions occurred repeatedly throughout the C Zone and Interlake areas suggesting that a common state of stress was present. Qualitatively resolving these observed directions into B Zone coordinates resulted in the orthogonal stress directions given in Table 3 and shown in Figure 10. These directions were used as the input parameters for the alternative numerical stress model; stress magnitude remained as per Table 2.

Table 3 Summary of C Zone stress orientation — with respect to B Zone mine grid

Principal stress		Trend (°)	Plunge (°)
Major stress	σ_1	070.0	15.0
Intermediate stress	σ_2	302.6	66.2
Minor stress	σ_3	165.0	18.0

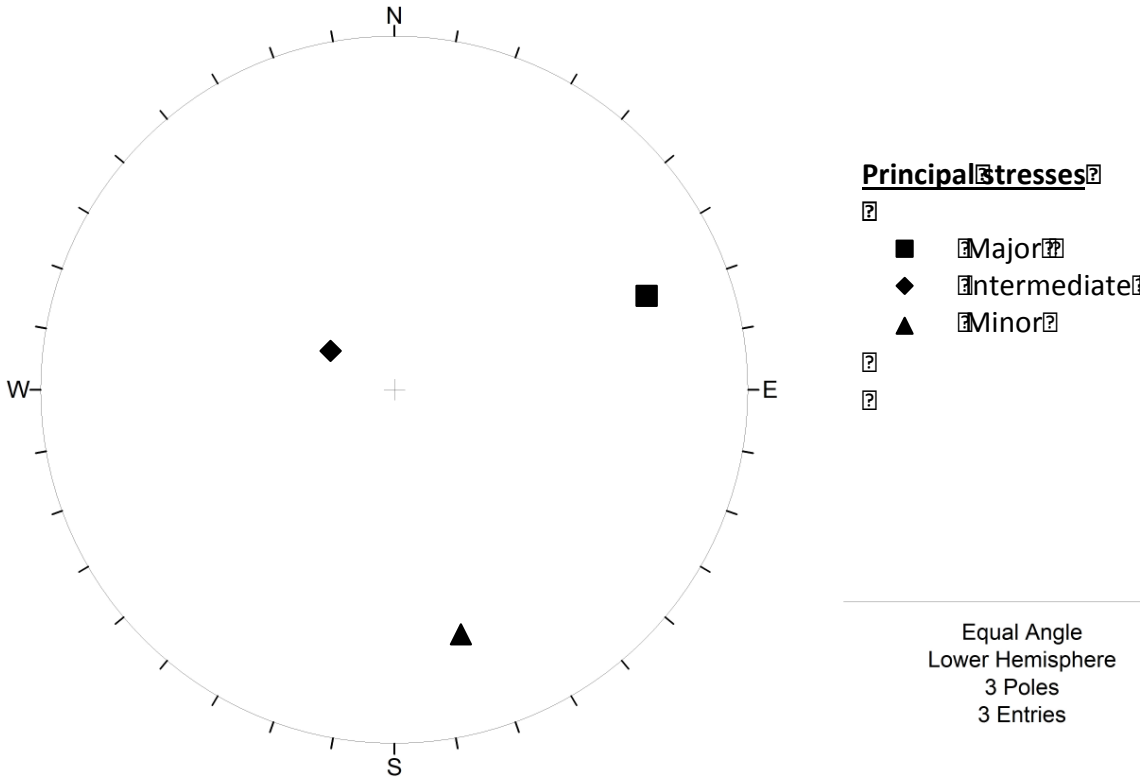

Figure 10 C Zone stress conditions — with respect to B Zone mine grid

3 Comparison of B Zone and C Zone stress models with seismic data

3.1 Comparison in a single region

The alternative stress model components given in Table 3 provided the second model variant for comparison to seismic moment tensor solutions. An elastic numerical stress model in monthly mining steps was created for one of the Interlake sill regions between 9,275 and 9,410 mRL, which was extracted between September 2013 and July 2014. The numerical model was evaluated first using the B Zone stress inputs from Table 2 then using the alternate C Zone stress inputs from Table 3.

In this period, a total of 1,906 seismic events were recorded, which were filtered for quality as per Section 2.4. The principal axes of source mechanisms (P-, B-, and T-axes), which are proxies of principal stresses σ_1, σ_2, and σ_3 respectively, were compared to the stress trajectories from the two model variants.

Figure 11 displays contours of maximum shear stress and trajectories of the major principal stress (σ_1) only for the B Zone stress inputs (old model) and the C Zone stress inputs (new model). Better correlation between the clusters of seismic events and regions of high shear stress can be clearly observed for the new model.

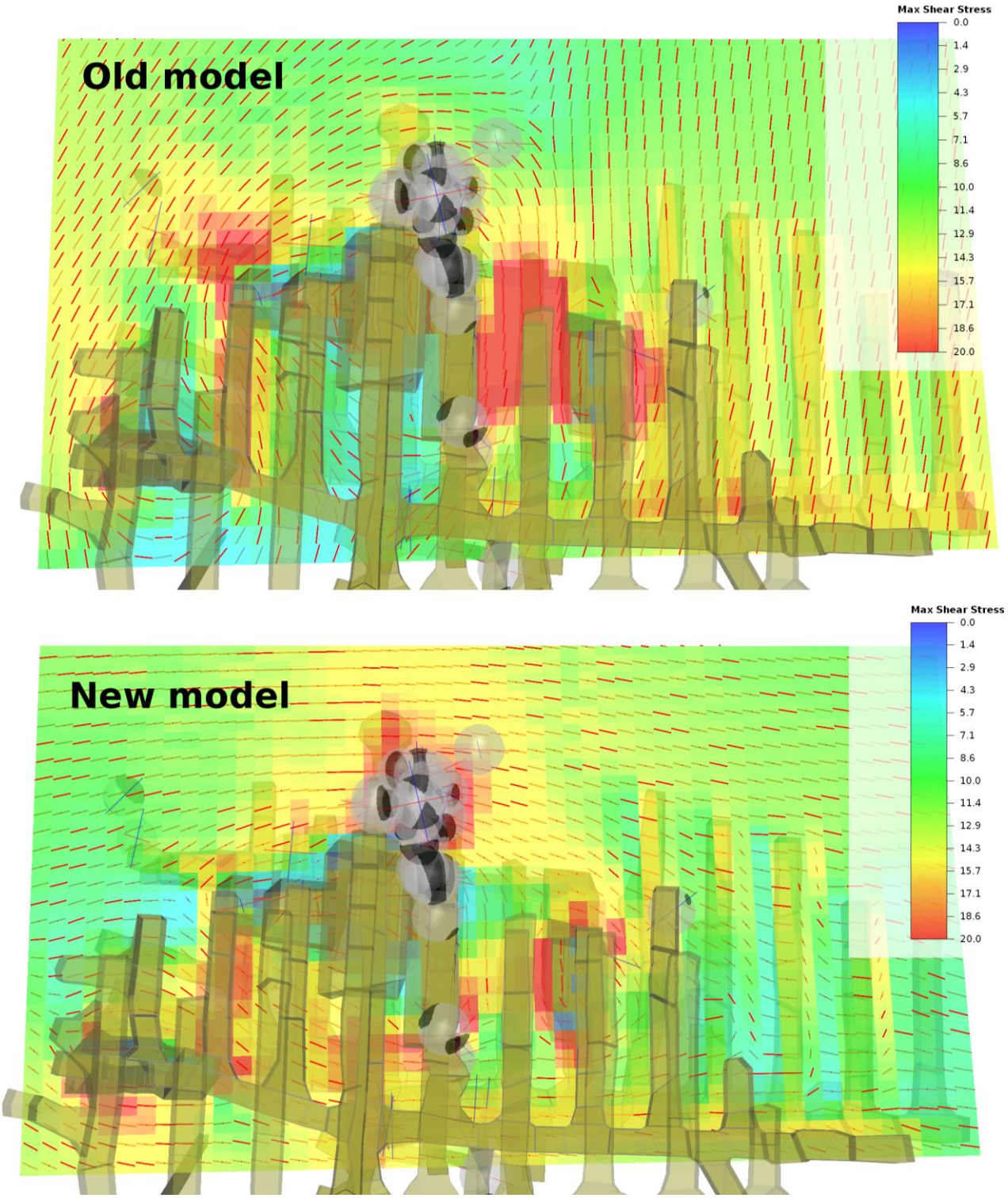

Figure 11 Directions of σ_1 (vector arrows) and magnitudes of maximum shear stress (contours) on the horizontal plane Z = 9,312 for both models of in situ stress

3.2 Comparison in multiple regions

The routine of comparing orientations of modelled principal stresses with the orientations of seismic mechanisms (P-, B-, and T-axes) was expanded to cover multiple regions in the same Interlake horizon for the same time period between September 2013 and July 2014. The regions are shown by the lightly shaded polygons in Figure 12.

Modelled stress trajectories were obtained for each principal stress component at each monthly model step and compared to the axes of principal seismic source mechanisms using stereonets. Comparison of the B Zone stress input parameters (old model) and the C Zone stress input parameters (new model) are shown in Tables 4 and 5 respectively. The C Zone model stress parameters derived from underground observations show a better agreement with seismic data for all mining regions when compared to those derived from extrapolated B Zone stress parameters; therefore it seems most likely that pre-mining stresses are orientated differently in C Zone/Interlake compared to B Zone.

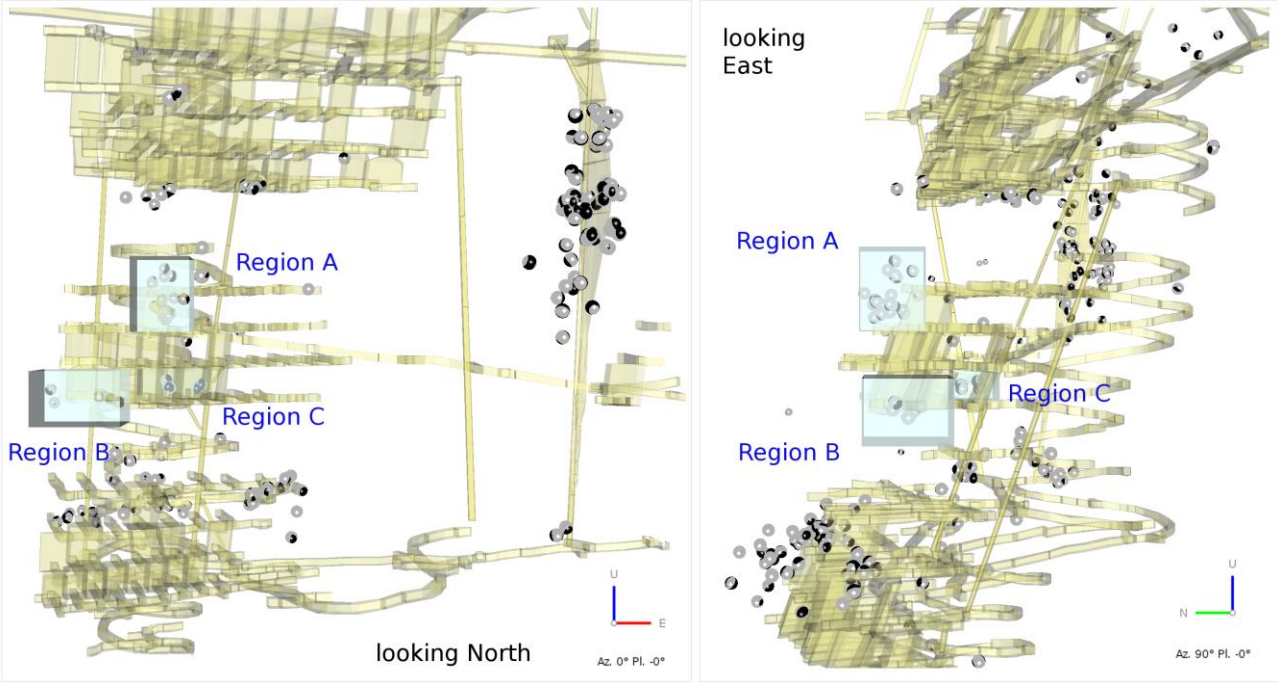

Figure 12 Detailed analysis regions for correlating stress models with seismic data

Table 4 Principal axes of stresses for the B Zone (old) model and source mechanisms

	Region	A	B	C
Major Principal Stress	Model	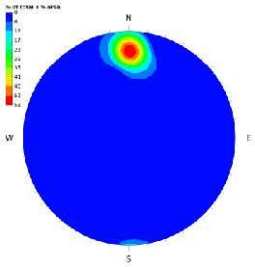	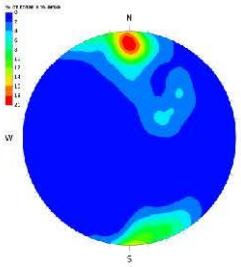	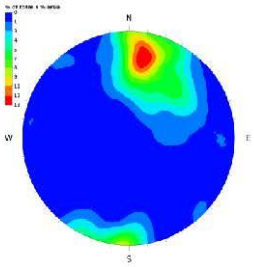
	Seismic proxy (P-axis)	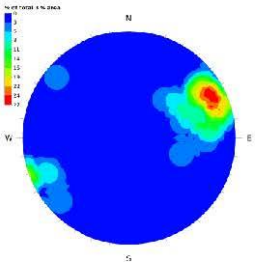	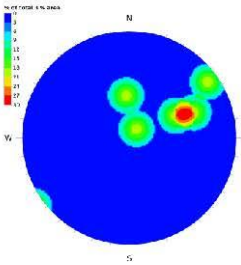	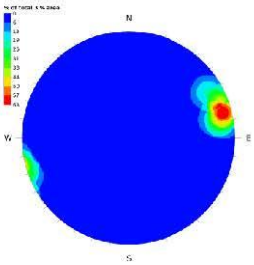
Intermediate Principal Stress	Model	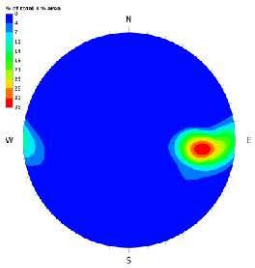	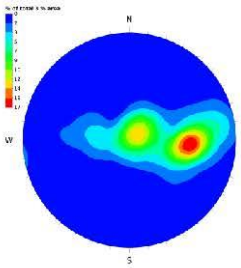	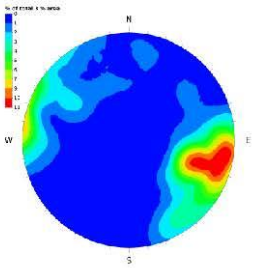
	Seismic proxy (B-axis)	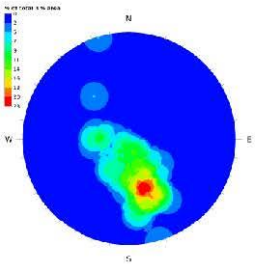	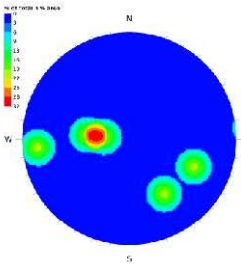	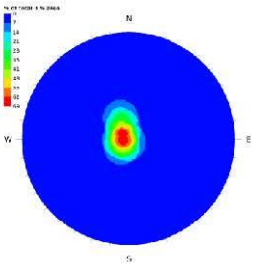
Minor Principal Stress	Model	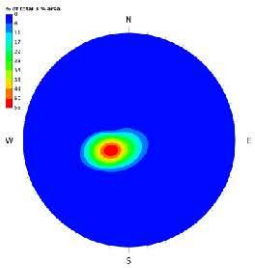	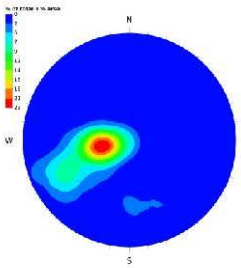	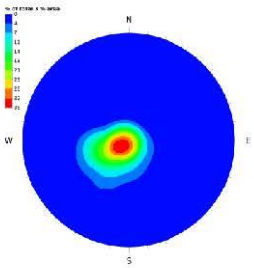
	Seismic proxy (T-axis)	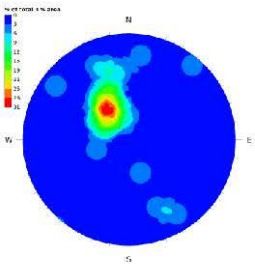	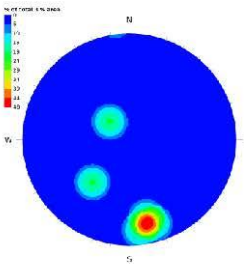	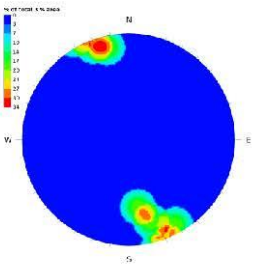

Table 5 Principal axes of stresses for the C Zone (new) model and source mechanisms

Region		A	B	C
Major Principal Stress	Model	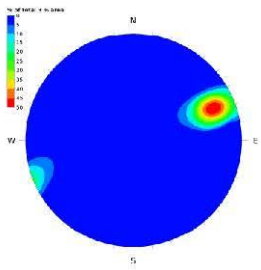	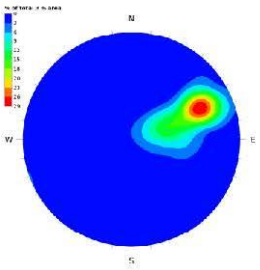	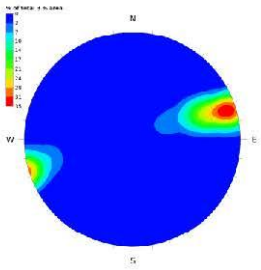
	Seismic proxy (P-axis)	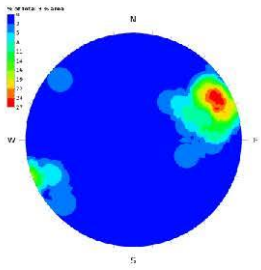	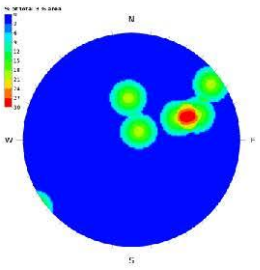	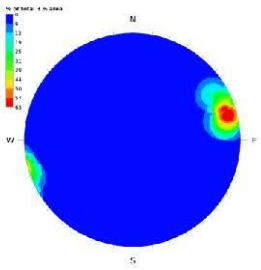
Intermediate Principal Stress	Model	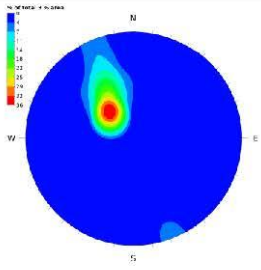	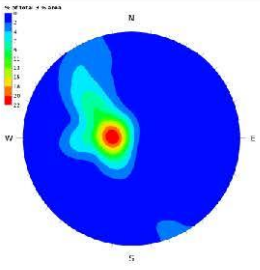	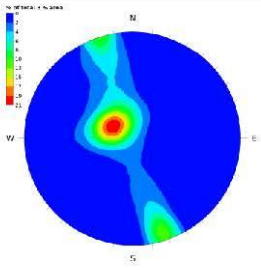
	Seismic proxy (B-axis)	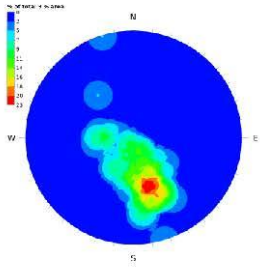	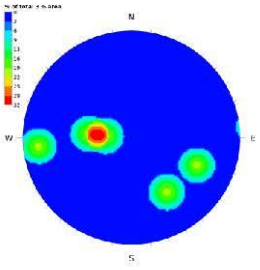	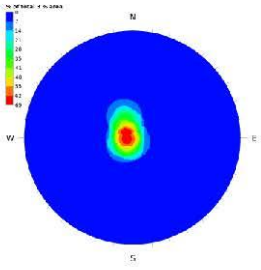
Minor Principal Stress	Model	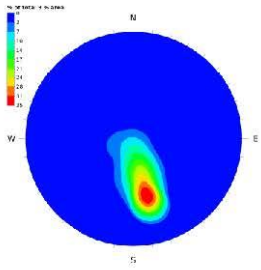	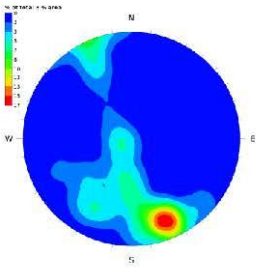	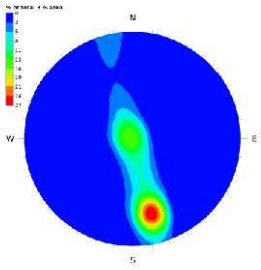
	Seismic proxy (T-axis)	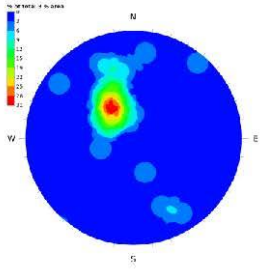	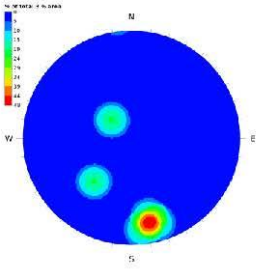	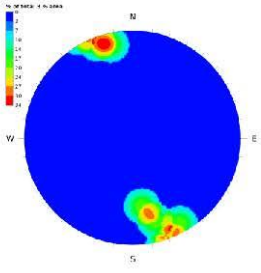

4 Discussion and conclusion

The first part of this paper highlighted some of the issues faced at an older mine with a complex ownership history, when ground behaviour of a newer production zone began to diverge away from established mine planning rules. This followed the principle of observation-led design, promoting routine back-analysis as a means to progress forwards. The conversion of all historical Hemlo data from its composite forms into a standardised system was an extensive side-project, but worth the effort for the huge catalogue of reference material that was made accessible to technical services personnel and vastly reducing the time needed to create numerical sub-models for prompt analysis of mining problems. The system layout also established the foundation framework for new data acquisition systems, which were critical in understanding the differences between mining zones, and which continue to be used to further refine stress model and rock mass failure criteria.

Comparing parameters of elastic stress models (maximum shear stress and orientation of principal stress axes) with seismic information (source locations and mechanisms) might be considered simplistic, but the results have worked favourably in these examples.

The seismic events recorded around OP7/OP7A were associated with stress fracturing. The location of events and principal axes of source mechanisms were in good agreement with the measured orepass profile, which proved to be a useful indicator of orepass wear during back-analysis and led to the analysis technique being expanded to other orepasses at Williams Mine. An additional benefit is that localised variations in stress directions can be investigated and individual results can be combined to characterise the lateral variation of the stress field along the entire extent of the Hemlo orebody strike. This project is currently ongoing at Williams Mine.

The repeatability of the technique within stoping areas, combined with high quality records of underground observations, made it possible to conclude that the model of in situ stress adopted from B Zone experience (major principal stress normal to the orebody strike) is not appropriate for the C Zone/Interlake regions. The proposed alternate model with major principal stress orientated sub-parallel to C Zone orebody strike better explains both underground observations and seismic data in the C Zone/Interlake orebody. Subsequent analysis of additional C Zone case studies provided the required confidence for the alternate model parameters to be used for routine C Zone mine design evaluation, with ongoing seismic monitoring continually supplementing factual observations of ground performance across the Hemlo complex.

Similar comparison of stress modelling parameters with seismic data can reasonably be attempted elsewhere provided significant difference exists between variants (as in the case between B Zone and C Zone). However, it is important to consider that regions of maximum shear stress provided by the elastic model may have already yielded before the analysed seismicity was recorded. Furthermore, P-, B- and T-axes of source mechanisms represent proxies of the three principal stress maximums under the assumption that strength of the rock mass can be considered isotropic and homogeneous. Where distinct planes of weakness exist, axes of source mechanisms can deviate from the principal stresses significantly and/or the weakness may be located outside the regions of maximum shear stress. Ideally, seismic events associated with specific weakness planes should be separated from the seismic data related to rock mass response.

When the difference between the alternative stress models is subtle, then other approaches may have to be used. One possible option is to explicitly model seismic response for each suspected stress case and compare it with the observed response in seismological terms (e.g. modelled sizes of events versus observed sizes, and modelled mechanisms versus observed mechanisms). This method of modelling mining induced seismicity was originally suggested by Salamon (1993) and elaborated further by Linkov (2005; 2013). It is a useful method because it accounts for inelastic deformation around the excavations and includes the effect of joint sets and weak faults. An example of this modelling technique applied to Hemlo data has also been described by Malovichko and Basson (2014).

Acknowledgement

The authors would like to acknowledge Barrick Gold Corporation, Hemlo Operations: Williams Mine, which kindly permitted the use of its data. Many thanks also to the geotechnical team and other members of the technical services department who assisted in this body of work.

References

Bawden, WF 2006, *February 2006 site review, Williams Operating Company & David Bell Mine*, internal report, p*repared for Barrick Gold*, Kingston, Canada.

Coulson, A 2009, 'Investigation of the pre to post peak strength state and behaviour or confined rock masses using mine induced microseismicity' PhD thesis, University of Toronto.

Kazakidis, VN 1990, 'An integrated study of fractured rock mass behaviour using structural mapping, microseismic monitoring and numerical modelling' Master of Science thesis, Queen's University.

Linkov, AM 2005, 'Numerical modeling of seismic and aseismic events in geomechanics', *Journal of Mining Science*, vol. 41, no. 1, pp. 14-26.

Linkov, AM 2013, 'Numerical modelling of seismicity: theory and applications', in A Malovichko & D Malovichko (eds*), Proceedings of the 8th International Symposium on Rockbursts and Seismicity in Mines*, GS RAS & MI UB RAS, Obninsk-Perm, pp. 197-218.

Malovichko, D & Basson, G 2014, 'Simulation of mining induced seismicity using Salamon-Linkov method', in M Hudyma & Y Potvin (eds), *Proceedings of the 7th International Conference on Deep and High Stress Mining*, Australian Centre for Geomechanics, Perth, pp. 667-680.

Malovichko, D & Lotter, E 2008, *Moment tensor inversion for Jmts (using amplitudes & polarities)*, internal report, prepared for ISS International, Stellenbosch, South Africa.

Mendecki, AJ 1993, 'Real time quantitative seismology in mines', in P Young (ed.), *Proceedings of the 3rd International Symposium on Rockbursts and Seismicity in Mines*, Balkema, Rotterdam, pp. 287-295.

Muir, TL 1997, *Precambrian geology, Hemlo Gold deposit area: volume 289 of Ontario Geological Survey report,* Ontario Ministry of Northern Development and Mines, Ontario, Canada.

Salamon, MDG 1993, 'Some applications of geomechanical modelling in rockburst and related research', in P Young (ed.), *Proceedings of the 3rd International Symposium on Rockbursts and Seismicity in Mines*, Balkema, Rotterdam, pp. 297-309.

van Aswegen, G 1993, 'Applications of quantitative seismology in South African gold mines', in P Young (ed.), *Proceedings of the 3rd International Symposium on Rockbursts and Seismicity in Mines*, Balkema, Rotterdam, pp. 261-266.